JGR Solid Earth

Key Points:
- Time-lagged magnetic pulsations ranged at 0.1–0.2 Hz are observed in a limited area
- Elliptical particle motion suggests dominant P-SV-type microseisms
- Time-lagged magnetic pulsations can be generated by the motional induction effect

Supporting Information:
- Supporting Information S1

Correspondence to:
C. H. Chen,
nononochchen@gmail.com

Magnetic Pulsations Triggered by Microseismic Ground Motion

Chieh-Hung Chen[1,2] [ID], Jing-Yi Lin[3] [ID], Yongxin Gao[4] [ID], Cheng-Horng Lin[5] [ID], Peng Han[6], Chun-Rong Chen[7] [ID], Li-Ching Lin[8] [ID], Rong Huang[2], and Jann-Yenq Liu[7,9,10] [ID]

[1]State Key Laboratory of Geological Processes and Mineral Resources, China University of Geosciences, Wuhan, China, [2]Institute of Geophysics and Geomatics, China University of Geosciences, Wuhan, China, [3]Department of Earth Sciences, National Central University, Taoyuan, Taiwan, [4]School of Civil Engineering, Hefei University of Technology, Hefei, China, [5]Institute of Earth Sciences, Academia Sinica, Taipei, Taiwan, [6]Department of Earth and Space Sciences, Southern University of Science and Technology, Shenzhen, China, [7]Department of Space Science and Engineering, National Central University, Taoyuan, Taiwan, [8]Department of System Engineering and Naval Architecture, National Taiwan Ocean University, Keelung, Taiwan, [9]Center for Astronautical Physics and Engineering, National Central University, Taoyuan, Taiwan, [10]Center for Space and Remote Sensing Research, National Central University, Taoyuan, Taiwan

Abstract Geomagnetic pulsations with an enhanced amplitude of 0.1–1 nT in a frequency band of 0.1–0.2 Hz were observed by three three-component magnetometers. The geomagnetic pulsations exhibit slight time difference that is unusually observed within a limited area of $\sim 5 \times 5$ km^2 at the northern end of Taiwan. The time difference suggests the geomagnetic pulsations are not dominated by global effects but local ones. We compare the seismic signals recorded by the cosited broadband seismometers for investigating potential mechanisms of these geomagnetic pulsations. Results from analysis of both seismic and geomagnetic data exhibit consistent source azimuths from the Pacific Ocean to the northeast of the observation sites with a wave propagation speed of ~ 2.9 km/s estimated based on P-SV-type microseisms. Polarization and particle motion analyses demonstrate that the geomagnetic pulsations move with an elliptical rotation form, showing a close association with the P-SV-type microseisms. The 90° phase difference between the horizontal and vertical components of the geomagnetic signals suggests that the time-lagged geomagnetic pulsations are possibly caused by the motional induction effect after the arrivals of P-SV-type microseisms.

1. Introduction

The primary aim of monitoring the geomagnetic field is to study the variations in the Earth's main field (Chapman & Bartels, 1940) and solar activity (Smith et al., 2004; Vassiliadis et al., 1990). When continuous geomagnetic data recorded by magnetometers located within limited areas are examined, synchronous changes with an insignificant time lag in those data are generally interpreted to be the result of global effects dominated by the interaction of variations in the Earth's main field with solar activity on a worldwide scale. However, on a local scale, the geomagnetic field can also be disturbed by ground motion (e.g., Breiner, 1964; Eleman, 1965; Gao et al., 2016; Yamazaki, 2012). Honkura et al. (2004) reported that P-wave arrivals could vary electric and magnetic fields near the surface. Although geomagnetic pulsations can be directly triggered by P waves (e.g., Breiner, 1964; Eleman, 1965; Tsegmed et al., 2000; Yamazaki, 2012), those pulsations are small and close to the amplitude of background noise (Guglielmi et al., 2004). Guglienlmi et al. (2004) recognized magnetic disturbances triggered by Love waves using a polarization method against background noise. On the other hand, disturbances to the geomagnetic field can also be either generated by Rayleigh waves due to ground motion induced by wave arrivals or excited by acoustic waves that are vertically propagating into the atmosphere and changing the electron contents in the ionosphere (Liu et al., 2016; Lognonné et al., 1998; Occhipinti et al., 2010). All the above-mentioned magnetic signals induced by the seismic waves are just local responses and restricted within the passage of the seismic waves. In contrast to the global effect, the geomagnetic changes reported above usually show significant time differences for the related signals retrieved from adjacent stations. The conversion from a seismic wave to a magnetic disturbance can be caused by several mechanoelectric mechanisms. Both theoretical modelings (e.g., Gao & Hu, 2010; Gao et al., 2016; Garambois & Dietrich, 2002; Haartsen & Pride, 1997; Ren et al., 2015) and laboratory
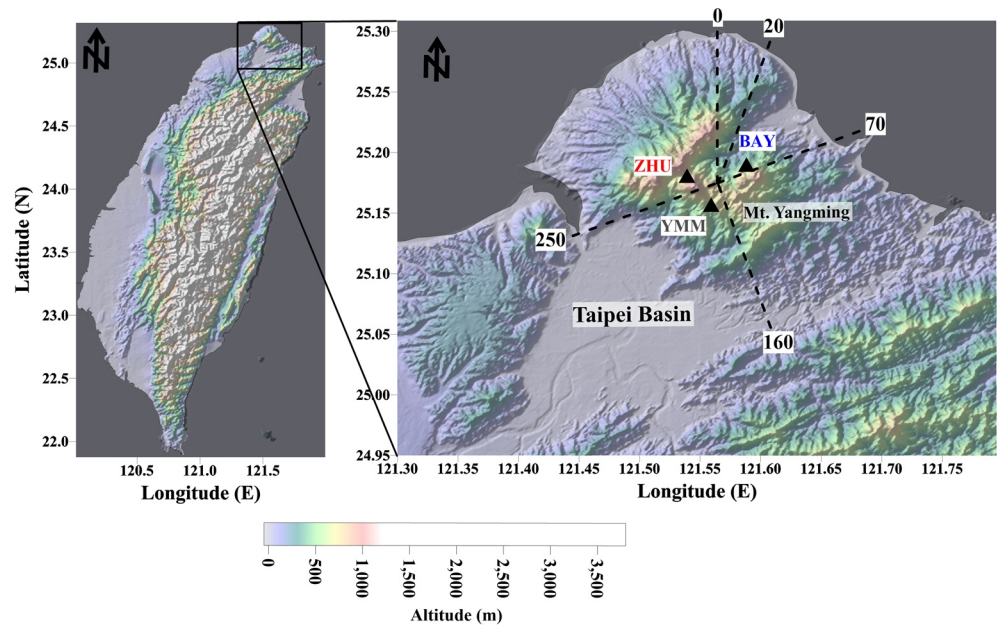
Figure 1. Locations of the magnetic and cosited seismic stations. The location of Taiwan area on a boarder scale is shown in the left panel. The locations of the magnetic and cosited seismic stations are denoted by black triangles shown in the right panel. The numbers at the ends of the dashed lines indicate the clockwise angles of rotation relative to the center of the three stations for reference.

experiments (e.g., Bordes, 2008) show that the electrokinetic effect (Pride, 1994; Revil & Linde, 2006) is an effective mechanism that can produce observable magnetic signals accompanying the seismic waves. Theoretical simulations also indicate that the motional induction effect (e.g., Gao et al., 2014, 2019) is the other viable mechanism. A magnetometer array on a local scale can be utilized to investigate the mechanism for the generation of magnetic disturbances that is beneficial for identifying or extracting possible factors which can interact with the geomagnetic field.

To routinely monitor changes in the geomagnetic field at the northern end of Taiwan, a three-component fluxgate magnetometer with a resolution of 0.01 nT and a sampling rate of 1 Hz was installed at the permanent station YMM (121.560°E, 25.155°N) in December 2012 (Figure 1). Two temporal stations (i.e., BAY (121.589°E, 25.188°N) and ZHU (121.540°E, 25.179°N)) with the same type of magnetometer were established to the northeast and northwest of the YMM station separated by distances of ~3–7 km between May and August in 2014 to enhance the monitoring capacity of the network (Figure 1). Consistent diurnal variations among these stations suggest that the magnetometers at the BAY, YMM, and ZHU stations operate normally (Figure 2a). The geomagnetic field in the nighttime (18:30–21:00 UT or 2:30–5:00 LT; determined as low-noise time hereafter) is quite stable relative to those observed during other periods throughout the day (also see Chen et al., 2017). To better estimate the reliability of the data, we constructed the confidence interval test by using the red noise spectra via the method proposed in Gilman et al. (1963) and Schulz and Mudelsee (2002). Figure 2b reveals that the product of the power spectrum density (computed by using the fast Fourier transform) multiplied by the frequency is significantly enhanced and exceeds the 80% confidence interval in the frequency band of 0.1–0.2 Hz at all three stations (BAY, YMM, and ZHU). This result indicates that there is truly an unknown source continuously dominating the geomagnetic field in the frequency band of 0.1–0.2 Hz at the northern end of Taiwan. Meanwhile, this frequency characteristic associated with these enhanced products for the geomagnetic data have rarely been reported or discussed in previous studies. After applying a bandpass filter between 0.1 and 0.2 Hz centered at 0.15 Hz to the geomagnetic records, variations of the filtered data at the three stations show a similarity in amplitudes and envelops varying along the time (Figure 2c). This suggests that the magnetic field in the frequency band of 0.1–0.2 Hz at the three stations is probably dominated by a source. We further examine changes of the filtered data within a time span of 64 s shown in Figure 2d and found slight time difference among the geomagnetic data recorded at the three stations. The time
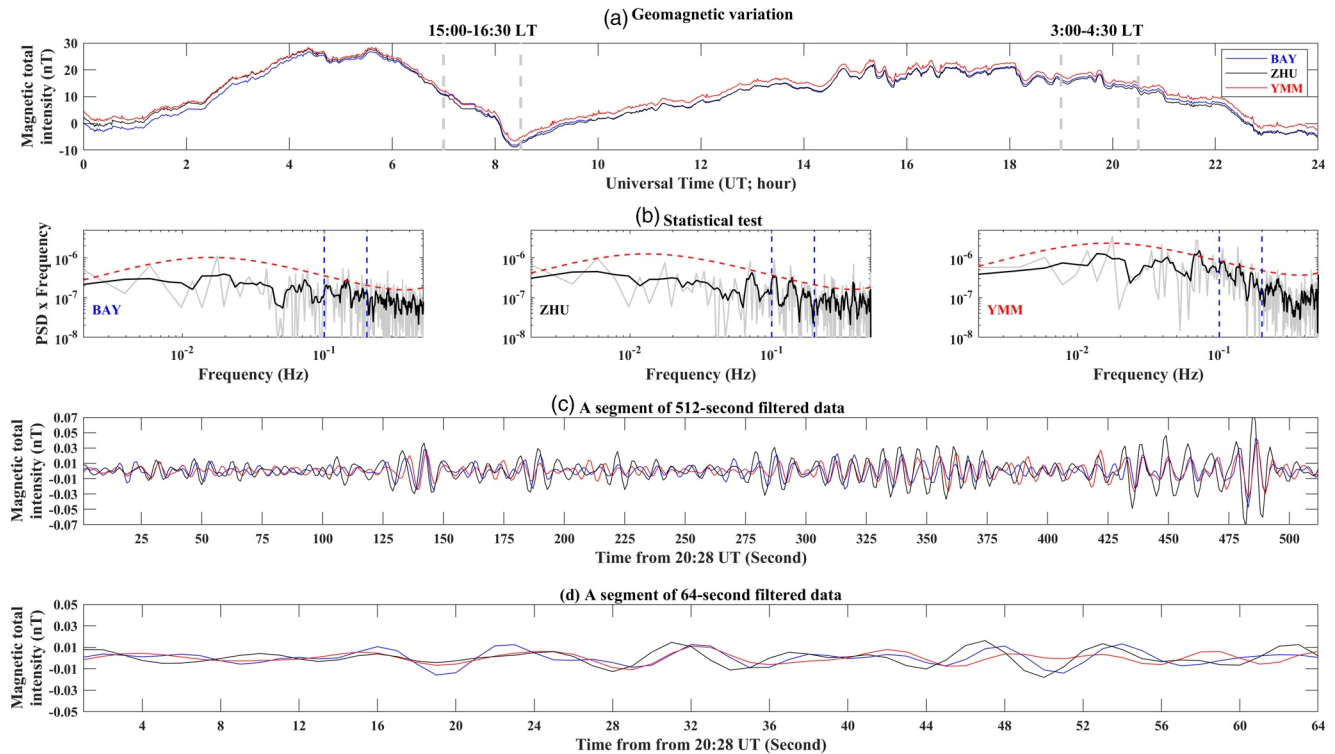
Figure 2. Variations and frequency characteristics of the geomagnetic field at the BAY, ZHU, and YMM stations on June 17, 2014. Red, blue, and black lines show the data from YMM, BAY, and ZHU, respectively. Variations in the geomagnetic total intensity field with a sampling interval of one minute to the first observation point on June 17, 2014, are shown in (a). Statistical test results are shown in (b). Gray lines indicate that the products computed by multiplying the power spectrum density (PSD) by the frequency vary with the frequency. The black lines denote the running average. The dashed red and blue lines indicate the 80% confidence interval determined by red noise (Gilman et al., 1963; Schulz and Modeless, 2002) and the boundaries at 0.1 and 0.2 Hz, respectively. Raw data with a segment of 512 and 64 s processed with a bandpass filter of 0.1–0.2 Hz are shown in (c and d), respectively. Note that influences from a difference between the first and the last samples of the raw data are mitigated by using a Tukey window before the filter.

difference indicates that unknown sources should come from the northern side of the stations sequentially dominating the geomagnetic field on a local scale due to a delay of magnetic wave arrivals at the YMM station. We investigated the northern side relative to the three magnetic stations and considered that the source should originate from oceans (also see Figure 1).

Microseisms, which are primarily generated by the coupling between ocean waves and the seafloor (e.g., Cessaro, 1994; Longuet-Higgins, 1950b), are the most common signals in seismograms at frequencies ranging between 0.05 and 0.3 Hz that are considered to be the promising source of the geomagnetic signals observed in this study. When these oceanic waves and/or oceanic oscillations propagate onto land, P-type and P-SV-type microseisms are generated, and these two mechanisms can be distinguished by examining the propagation velocity and particle motion. The velocities of P-type microseisms are ∼6 km/s based on several investigations (e.g., Gualtieri et al., 2015). In contrast, the velocities of P-SV-type microseisms dominated by the fundamental mode are generally between ∼2.5 km/s and 4 km/s (e.g., Cessaro, 1994; Kimman et al., 2012). The concentration of magnetic energy at the frequency band (0.1–0.2 Hz) is in agreement with the frequency characteristics of microseisms. Here, we intent to reveal the potential sources and causal mechanisms of these time-lagged geomagnetic signals at this frequency band by analyzing the propagation process of the signals and its relation with the seismic data.

2. Data and Methodology

In this study, three-component geomagnetic data retrieved from the BAY, YMM, and ZHU stations between May and August in 2014 were examined to investigate the possible mechanism which induces the geomagnetic pulsations in the frequency band between 0.1 and 0.2 Hz. Ground motion monitoring by utilizing

cosited broadband seismometers was also conducted to facilitate a comparison between the magnetic and seismic data. The frequency-wavenumber (FK) method is a standard array technique, which simultaneously calculates the power distributed among different slownesses and directions of approach, and is widely used in the field of seismology (Capon et al., 1969; Goldstein and Archuleta, 1991a, 1991b; Schisselé et al., 2004). Whenever time delays of the signals recorded at different array stations, we can utilize the summation of the coherent data stream from each station to improve the signal-to-noise ratio (SNR) for a specific phase that brings the signals into phase and provides a direct estimate of the back azimuth and the slowness of the particular signal. Thus, this method has also been applied for other kind of wavefield data analysis, such as acoustic signals. With the FK method, single-component data from an array are processed using a bandpass filter to estimate the time-varying energy within a particular band via the Fourier transform. To increase the reliability of our results, the FK analysis software developed by Riahi et al. (2014) and Riahi and Saenger (2013) is utilized (https://github.com/nimariahi/fk3c), which extended to additionally decompose polarizations for three-component data from an array that allows more sensitive detection for the source direction and a much more precise estimation for the surface wave anisotropy. In practice, we applied the source code of the three-component FK analysis to the 3-component magnetic data and cosited broadband seismometer data to further investigate the back azimuth and the slowness of potential waves that cause the time difference magnetic pulsations in the northern end of Taiwan.

In this work, geomagnetic data recorded early in the morning during a low-noise time (i.e., 19:00–20:30 UT or 3:00–4:30 LT) were chosen and used for further analyses to avoid the influence of artificial noise (Chen et al., 2017). Furthermore, geomagnetic data recorded at a noisy time in the afternoon (6:00–7:30 UT or 15:00–16:30 LT) were also analyzed as a reference to understand the influence of artificial noise on the geomagnetic field. Both geomagnetic (including low-noise and noisy time data) and seismic data were filtered by using a bandpass filter that was centered at 0.15 Hz. These filtered data with a duration of 1.5 h were processed by the three-component FK method with a window of 64 s and a step of one and a half window lengths (i.e., 96 s). To avoid temporary influence from the environment disturbance to the magnetic field, we first applied the wavelet-based semblance analysis (Cooper & Cowan, 2008) on our data to examine how coherent the magnetic data in a window is between any station pair. The semblance analysis gives ratios between the energy of the stack signals and the sum of the energy of the single traces which could be an indicator for the adaption of the three-component FK analysis. Figure 3 shows an example of the semblance ratios calculated from the magnetic data in Figure 2d. The semblance ratios obtained from every two stations exhibit median values of 0.91, 0.82, and 0.75 in the frequency band of 0.1–0.2 Hz. These suggest that variations of the magnetic data at three studied stations are similar in this particular frequency band during the recorded time. Once the semblance ratios obtained from the data in a window are larger than 0.7, the three-component FK analysis are utilized for the FK analysis.

3. Results

After applying the FK analysis for all the data segments, we can obtain the propagation azimuth versus to wavenumber distribution pattern for the magnetic energy concentration. One example of the spectrum computed from the filtered magnetic data by using the three-component FK analysis is shown in Figure 4. Even though some relatively small spectra can also be observed at distinct azimuths. The dominating magnetic fields seems to be originated mainly from ~70° with a wavenumber of ~0.07 km^{-1} (~13.5 km/s in velocity), ~215° with a wavenumber of ~0.14 km^{-1} (~6.7 km/s in velocity) and ~55° with a wavenumber of ~0.31 km^{-1} (~3.0 km/s in velocity). The Tatun volcanic area is composed by basalts and andesites (C. H. Chen, 1978; Shellnutt, 2014). Thus, a P-wave velocity of 5.5 km/s and higher is assumed for the area (Christensen & Mooney, 1995). The phase velocity of the Rayleigh wave for a frequency range between 0.1 Hz and 0.2 Hz can be expected to be between 2.6 and 3.1 km/s based on the one dimensional reference model for the Tatun volcanic area by Pu et al. (2020). If we assume that the magmatic pulsations are caused by the microseismic activity, the velocity should not be as or higher than 6 km/s. Therefore, only the velocity ranged between 2.6 km/s and 3.1 km/s estimated from the FK analysis is consistent with the velocity of P-SV-type microseisms. This coincidence shows that magnetic pulsations and microseisms may indeed have some causal relationships. The azimuths of about ~55° could be the potential sources direction which triggers the geomagnetic pulsations observed in this study.
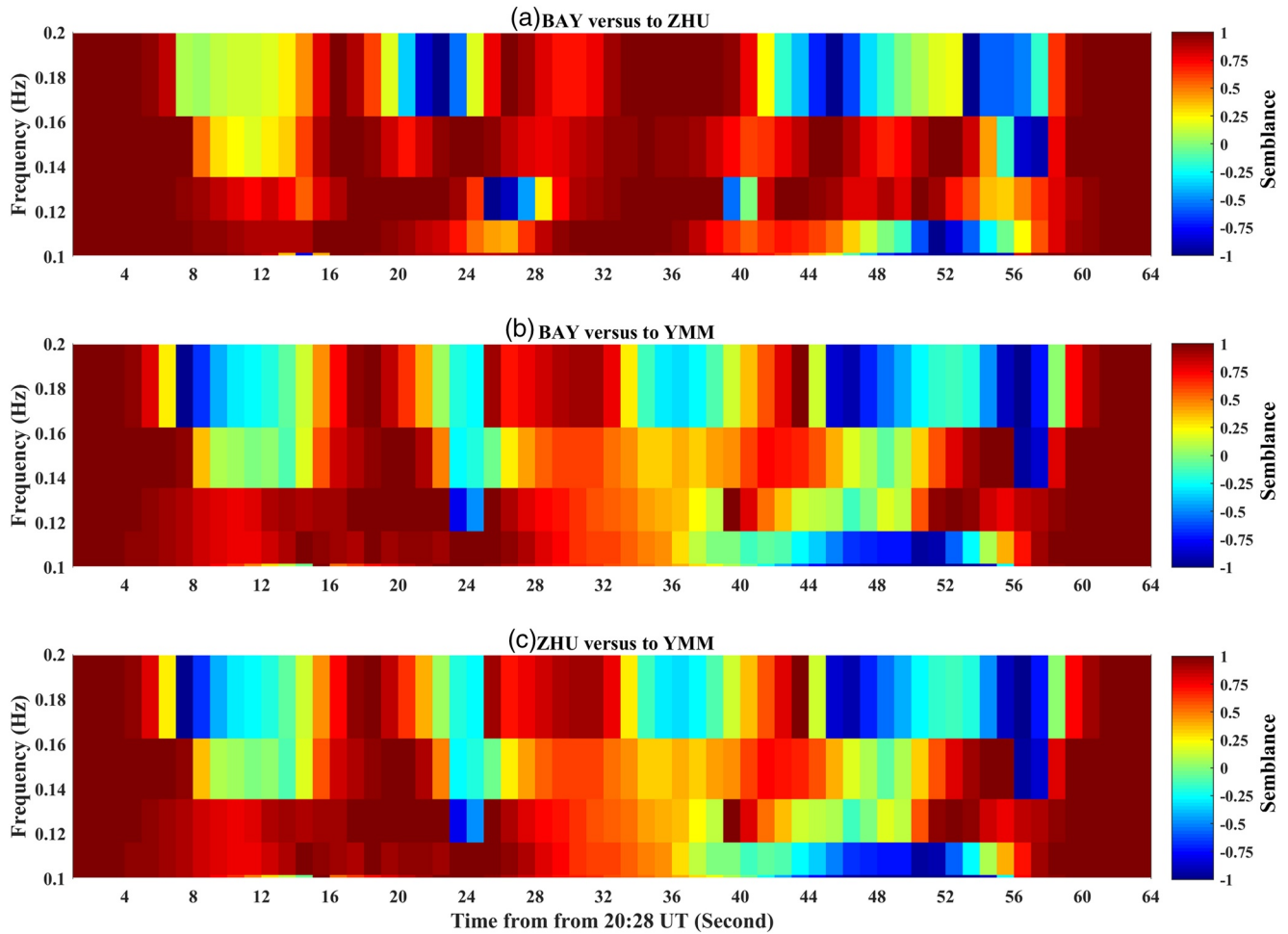
Figure 3. The semblance ratios among the magnetic data at three stations. Panels (a–c) show the semblance ratios of the magnetic data from the BAY versus to ZHU, BAU versus to YMM, and ZHU versus YMM at the frequency between 0.1 and 0.2 Hz, respectively. The color indicates the semblance ratios ranged between −1 and 1.
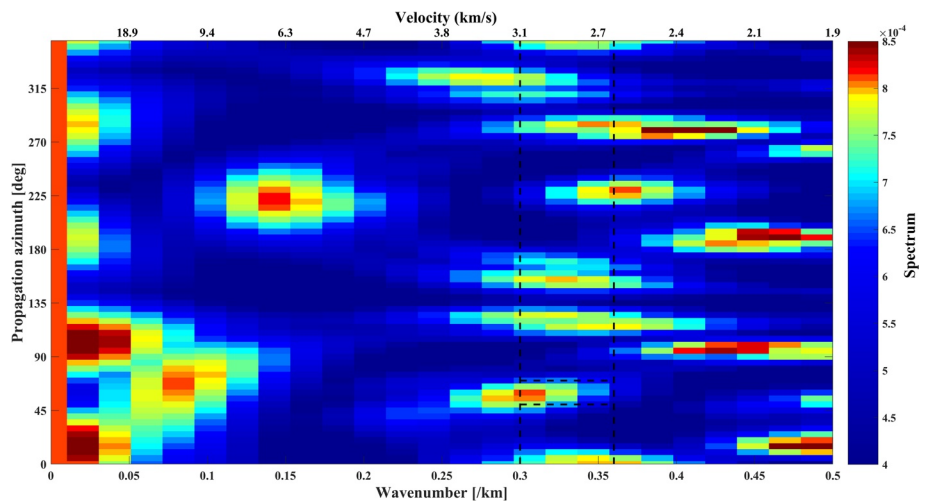
Figure 4. The spectrum distribution obtained from the magnetic data in Figure 2d using the three-component frequency-wavenumber analysis. Two vertical dashed lines indicate the velocity of the P-SV type ground motion at 2.6 and 3.1 km/s in the northern end of Taiwan. Two horizontal dashed lines surrounded azimuths of potential sources.
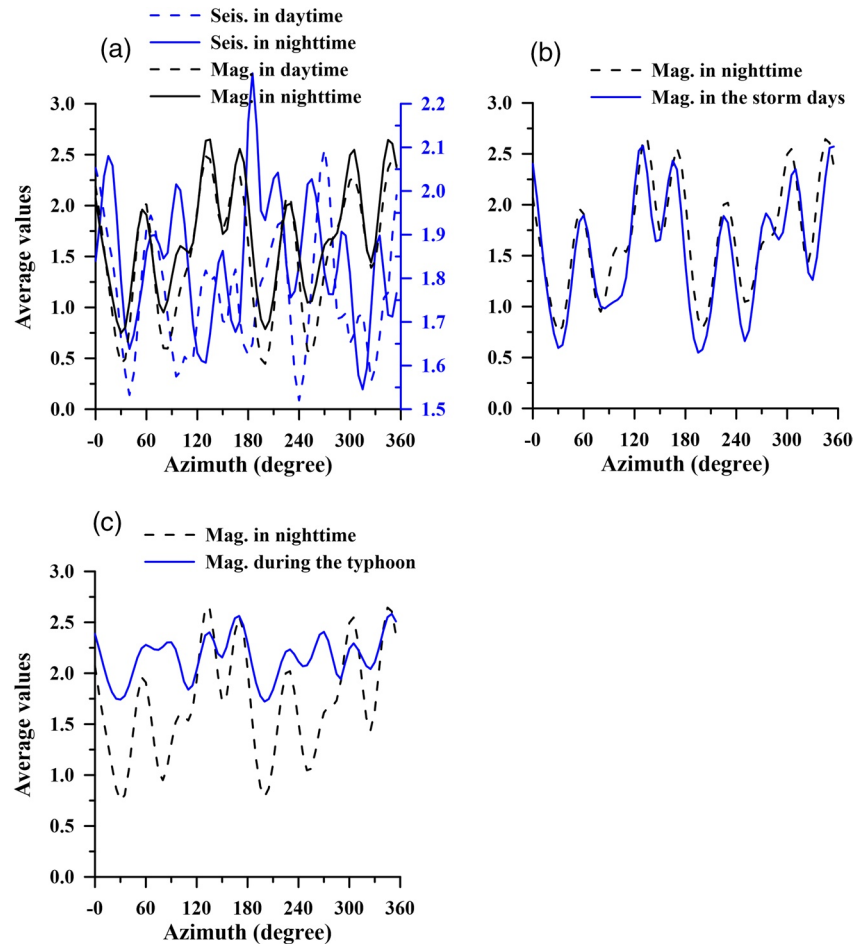
Figure 5. The average values of the normalized spectra from the geomagnetic and seismic data. The average values versus to the azimuth of wave propagations from the geomagnetic data and seismic data are shown in (a). The average values of the geomagnetic data during June 8–10, 2014 for the magnetic storm are shown in (b). The average values of the geomagnetic data during July 21–24 in 2014 for the typhoon impacting on Taiwan are show in (c).

To further examine the relationship between the magnetic and microseismic data, the FK results obtained from continuous seismic data recorded at cosited broadband seismometers are also calculated to perform the comparison between the two data sets. The seismic data were processed by using similar method as the magnetic data. Then, we normalized the spectrum results between the 2.6 and 3.1 km/s velocity band by dividing the maximum value of the amplitudes in each study window. Figure 5a shows the distribution of the average values of the entire normalized spectra versus to the azimuths from the noisy (i.e., daytime) and low-noisy (i.e., nighttime) data during the entire study period. The comparable distributions of the average values between the noisy and low-noisy data for the magnetic data suggest that disturbances on the geomagnetic field are permanent in the northern end of Taiwan, except for the azimuth at 105°. The exception would be caused by that weak signals are relatively easier to be detected in the low-noisy period. We further took the distribution derived from the ground motion data (i.e., seismic data) recorded on the geomagnetically quiet day (i.e., May 26, 2014) into consideration via the same method and parameters to examine the relationship between the time-lagged geomagnetic pulsations and microseisms. The average values for the azimuths from the ground motion and the magnetic data that are out of phase, except for the azimuth of ∼60°. This suggests that the magnetic data and the ground motion share a source from the azimuths of ∼60°. In general, the ground motion and geomagnetic data are affected by different mechanisms. Thus, the similarity in the propagation azimuth and the frequency content for both the geomagnetic pulsations and the microseisms may infer a causal relationship between the ground motion and the geomagnetic field. Chen et al. (2011) observed the azimuth range (i.e., 20–70°) of microseisms at the north end of Taiwan

that is in an agreement with the distribution of waves propagating of ∼60°. To verify the reliability of this result, we further compute the equivalent sources of microseisms by utilizing the frequency spectrum of the second order pressure data, which has main contribution to acoustic and microseisms through the global model of seismic noise energy radiation (Ardhuin et al., 2011; Hasselmann, 1963; Longuet-Higgins, 1950a). The major sources of microseisms do come from the direction near 60° to the northern end of Taiwan (Figure S2) that is in agreement with the shared azimuth at ∼60° in this study.

4. Discussions

(1) Possible origins for the magnetic pulsations at the 0.1–0.2 Hz frequency

Generally, abnormal geomagnetic signals on a worldwide scale are related to the occurrence of ionosphere storm. Thus, we utilized geomagnetic data during a magnetic storm (i.e., June 8–10, 2014) that is determined by the Dst index from the World Data Center for Geomagnetism, Kyoto to examine whether the permanent time-lagged geomagnetic pulsations and solar activities are independent. An agreement was found between the azimuth distributions derived from the data over the entire study period and from the data during the storm (Figure 5b). This result suggests that the geomagnetic pulsations observed in this study are irrelevant to the global effects; rather, they are dominated by a local phenomenon.

The great electrical conductivity contrast between ocean water and land can obviously dominate vertical magnetic fluctuations near coast lines that is well-known and is called the geomagnetic coast effect (Hitchman et al., 2000; Parkinson & Jones, 1979). We compute the Parkinson vectors from the geomagnetic data at the YMM station and find the vectors mainly direct toward 270° for the frequency at 0.1–0.2 Hz (Figure S1). The direction of the Parkinson vectors is significantly different with 60° that is the propagation azimuths of the geomagnetic pulsations observed in this study.

Typhoons are often considered an important source of microseisms. During the recording period of the magnetic network, Typhoon Matmo impacted Taiwan during July 21–24, 2014. The azimuth distribution of the geomagnetic pulsations changed accordingly and mainly distributed in ranges of 60–120° (Figure 5c). The equivalent sources of microseisms on July 22 are mainly located at the southeastern side of Taiwan where are the directions of near 90° to the northern end of Taiwan due to the typhoon (Figure S3). The agreement suggests that the geomagnetic pulsations observed in this study are relate to microseisms generated from the ocean. It should be noted that the effect of typhoon itself on the ionosphere change is not in this frequency band (Chen et al., 2014). This is the reason that we can link our reservation to the microseisms.

Note that previous studies (Gregori & Lanzerotti, 1980) reported that fluctuations of the geomagnetic field on the vertical component can be contributed from the result of local induction due to the inhomogeneous underlying electrical conductivity structure. A phase difference between the vertical and horizontal component of the geomagnetic field is often observed at a site. Although the phase difference caused by the local induction cannot be entirely removed, variations of microseism propagation azimuth during the typhoon can be utilized for further examination. If the propagation azimuths of the geomagnetic pulsations computed by using the phase difference are dominated by the local induction effect, the azimuths should be static during the study period of about 3 months due to unlikely changes of underlying electrical conductivity. However, the azimuths changed accordingly when the typhoon moved close to the eastern side of Taiwan (Figure 5c). This suggests that the local induction effect can be excluded from candidates that originates the geomagnetic pulsations. Thus, we suggest that the geomagnetic pulsations in the frequency band centered at 0.15 Hz observed in northern Taiwan are mainly induced by the ground motion on the local scale.

(2) The mechanism for the generation of geomagnetic pulsations

In the previous session, we compared various possible origins for the generation of geomagnetic pulsations observed in our study and we resumed that microseisms should be the most possible source. In this session, we intent to explore the mechanisms behind it. Figure 6 shows the particle motion of the seismic data and the polarizations of the observed geomagnetic pulsations. We can notice that both the particle motion and the polarizations demonstrate mainly elliptical rotation form movement. Thus, this similar motion pattern between the two data sets suggests that the geomagnetic pulsations should be triggered by ground motion
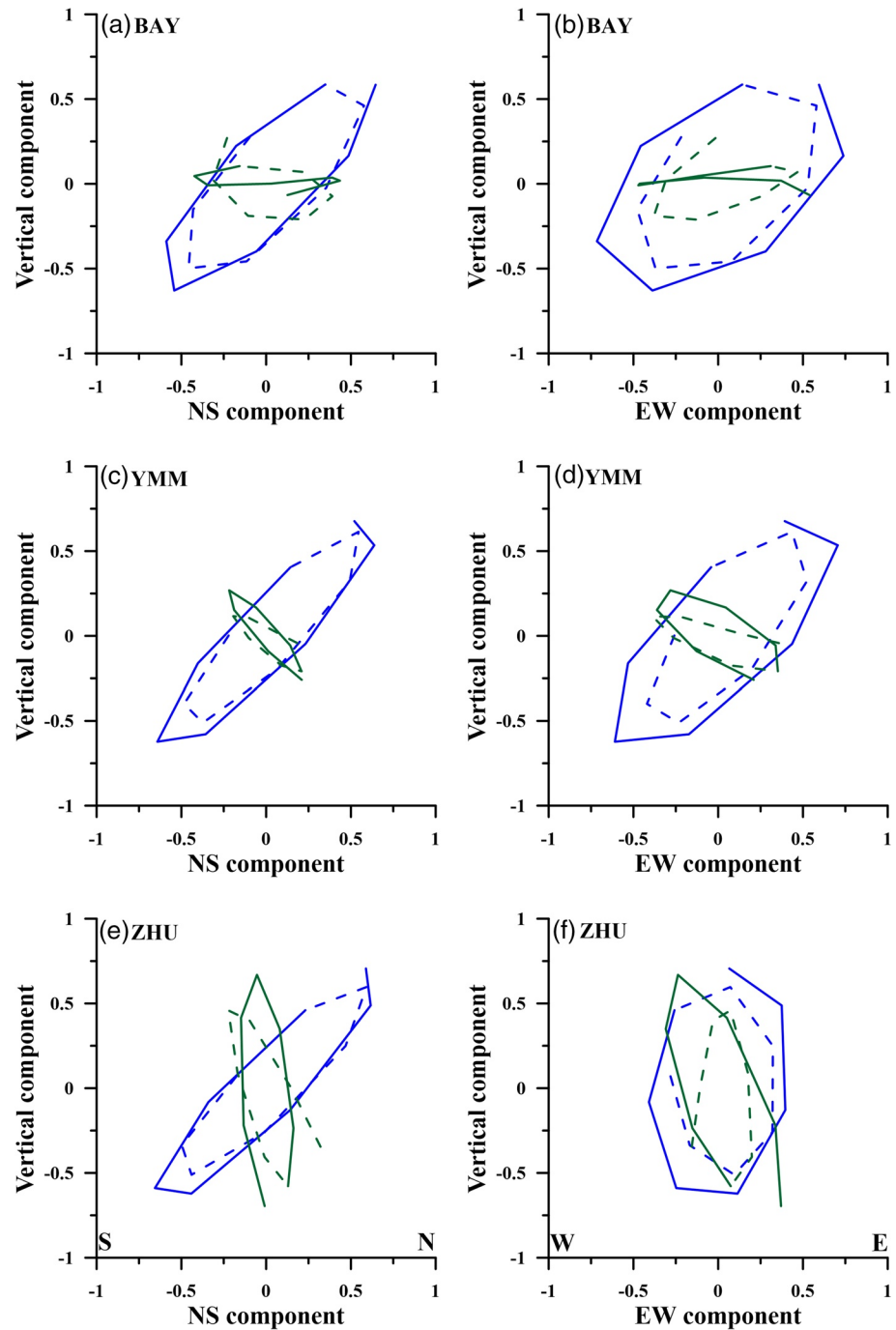
Figure 6. Particle motion of seismic waves and polarization of geomagnetic pulsations. Blue and green colors denote geomagnetic (unit: nT) and seismic data (unit: cm), respectively. The left (right) panel shows data on the NS (EW) component versus data on the vertical component. The dashed and solid lines indicate data from 1 to 6 s and 6–12 s, respectively. EW, East-West.

which are most likely the P-SV-type microseisms that originated from the Pacific Ocean. Geomagnetic pulsations could be directly triggered by P-SV-type ground motion due to the wave arrivals (Guglielmi et al., 2004; Honkura et al., 2004; Yamazaki, 2012) and/or an induction of acoustic-gravity waves from the motion upward propagating into the ionosphere changes in the electron contents (Artru et al., 2004; Hao et al., 2013; Liu et al., 2016; Occhipinti et al., 2011; Rolland et al., 2011). We evaluated the time difference between the geomagnetic pulsations and ground motion using the cross-correlation function (CCF) method, which is
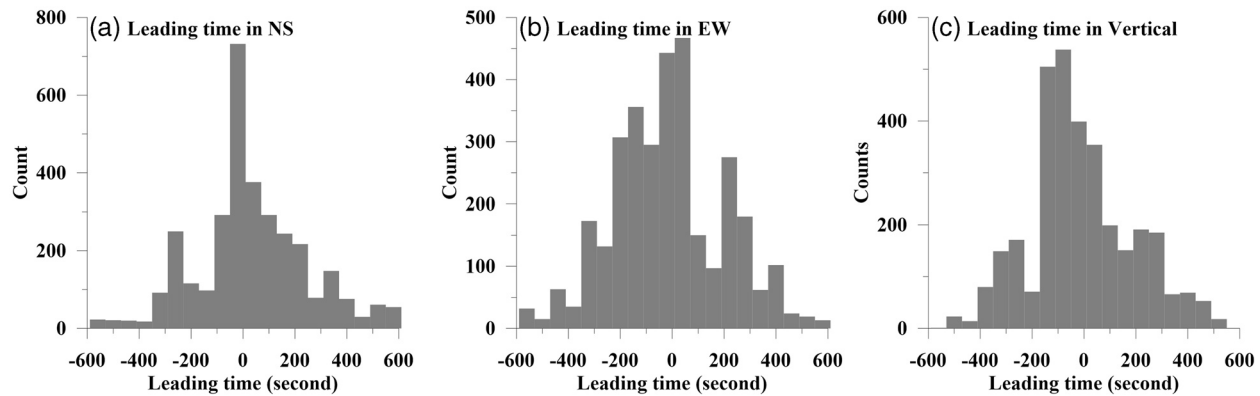
Figure 7. Lead times of the propagating geomagnetic waves relative to ground motion. The upper (bottom) panel shows the propagation velocities (lead times). Distributions of the lead times of magnetic pulsations relative to ground motion were obtained via the CCF method and are shown in (a–c). CCF, capital cash flow.

commonly used to estimate the time lag between continuous records from two wave sensors resembling impulse responses between them (Shapiro & Camille, 2004; Snieder, 2004; Weaver and Lobkis, 2001, 2002). If the geomagnetic pulsations are directly triggered by the ground motion, zero-time lags would be obtained. In contrast, once the variations in the geomagnetic field observed are excited by acoustic-gravity waves, seismic waves that lead geomagnetic pulsations by ∼4 min can be expected (Liu et al., 2016). The zero-time lags shown in Figures 7a–7c suggest that the geomagnetic pulsations observed in this work were not caused by changes in the electron contents but by the arrival of ground motion.

Even though the ground motion and the geomagnetic pulsations data demonstrate a good consistency in propagation pattern which indicates a strong link between them. Other factors, such as the tilt changes of the magnetometers caused by the seismic ground motion (i.e., the shaking effect), cannot be ignored. We retrieved the tilt change data of magnetic sensors from a tiltmeter assembled in the magnetometers and examined frequency characteristics using the red noise spectra again (Figure S4). Enhancements of the tilt change in a frequency band of 0.1–0.2 Hz can be found in the entire station. The amplitude of the tilt change in the frequency band is about 0.2–0.3 s (unit: degree). We estimate magnetic disturbance from the tilt changes through the roll pitch yaw angle (Slabaugh, 1999; also see supplementary). Amplitude of the disturbance is about 0.06 nT that is insufficient to directly contribute to the magnetic pulsations (0.1–1 nT) observed in this study. In fact, the tilt change mainly distributes in a frequency band of 0.4–0.5 Hz that is relevant to the amplitude of about 0.3–0.4 s. If the tilt change can amplify disturbance on the geomagnetic field, geomagnetic data can accordingly exhibit enhancements in the frequency band of 0.4–0.5 Hz. However, obvious enhancements of the geomagnetic data are not observed in the frequency band of 0.4–0.5 Hz but 0.1–0.2 Hz (Figure 2). This suggests that the geomagnetic pulsations observed in this study are not caused by the tilt changes.

In addition, if the geomagnetic pulsations are resulted from the tilt changes of the shaking effect, their horizontal and vertical variations should have same phase (i.e., no delay). To evaluate this possibility, we subsequently computed the phase differences between the horizontal and vertical magnetic fields and the phase differences between the horizontal magnetic field and horizontal seismic displacement (Figure 8). Only the analytical results associated with the EW and vertical component data are evaluated in Figure 8 because no significant relationship was obtained from the NS component data. This discrimination should be caused by the propagation direction of microseisms, which may decrease the magnitude of observed geomagnetic signals along the NS direction. The upper panel of Figure 8 shows that the phase differences between the EW and vertical magnetic fields are mainly distributed in the ranges of 45–90° for the BAY station and 75–120° for the YMM station, and the phase difference is ∼80° for the ZHU station. The lower panel of Figure 8 shows that the phase differences between the EW magnetic field and the EW particle displacement for the three stations are widely distributed. However, one of the major peaks appears at the phase difference of ∼90°. A phase difference that deviates from 90° would correspond to other mechanisms, whereas a phase difference near 90° demonstrates that the magnetic pulsations observed in this study are
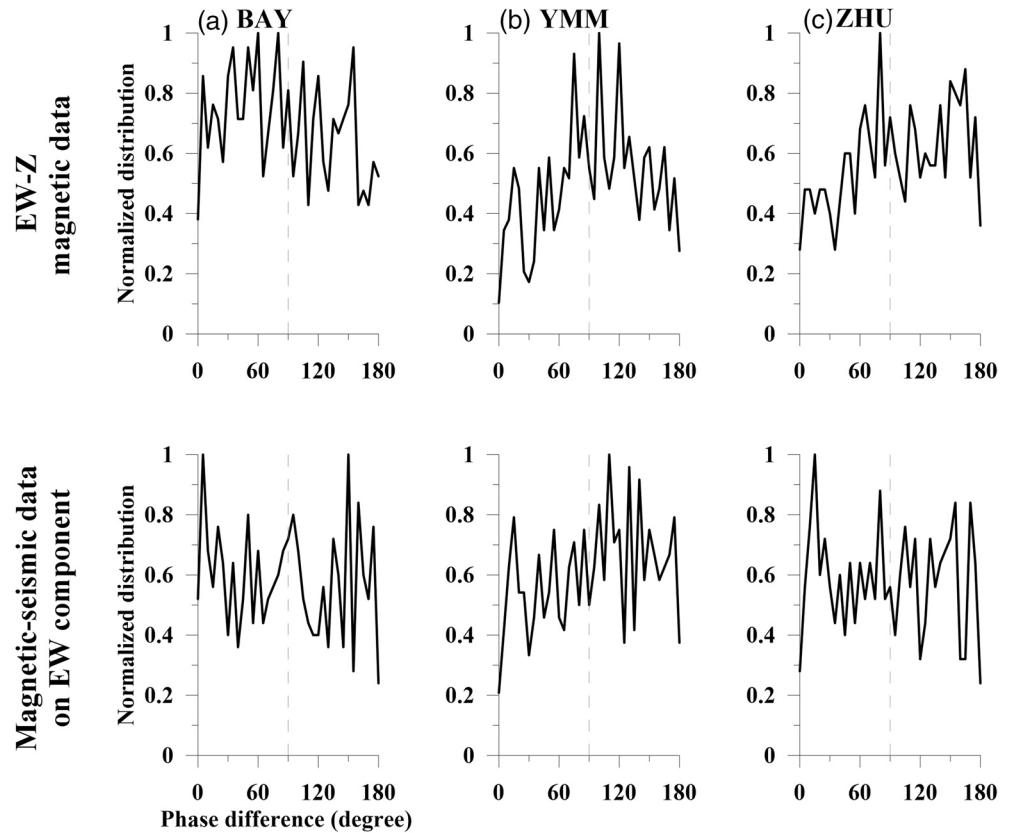
Figure 8. Normalized distributions of the phase differences between magnetic pulsations and ground motion during the low-noise period on the geomagnetically quiet day (i.e., May 26, 2014). Normalized distributions of phase differences with a resolution of 5° at BAY, YMM and ZHU are shown in (a–c), respectively. The upper panel shows the phase difference between the EW and vertical components within the geomagnetic data. The lower panel shows the phase difference between the geomagnetic data and ground motion on the EW component. Vertical dashed lines indicate a 90° phase difference. EW, East-West.

actual signals. Therefore, the time-lagged magnetic pulsations corresponding to the P-SV-type microseisms (also see Figure 7) in the frequency band of 0.1–0.2 Hz can be distinguished even though microseisms are generally considered to be weak and interact with many unknown ground motion sources.

The electrokinetic effect (Gao & Hu, 2010; Haartsen & Pride, 1997) and the motional induction effect (Gao et al., 2014, 2019) are two major potential mechanisms for the generation of a magnetic field accompanying seismic waves. We simulated electromagnetic signals generated by an earthquake source based on the motional induction effect using a 4-layer conductivity structure from C. S. Chen (2008) through the method proposed in Gao et al. (2019) (Figure S5). Simulation results show that the magnitude of the induced magnetic field is about 0.15 nT for the particle velocity of ground motion on the order of 0.01 m/s (Figure S6). The simulation results roughly agree with the observation shown in Figure 6, where the estimated velocity for the particle motion is in the order of ∼0.01 m/s while the magnetic signal is on the order of 0.1–1 nT. In addition, the simulation results show that the phase between the horizontal and vertical component of the simulated magnetic signal exhibits a difference of ∼90°. The phase difference between the horizontal magnetic signal and horizontal particle displacement is also ∼90° (Figure S6). Agreements between these properties and the motional induction simulations implies that the time-lagged magnetic pulsations associated with P-SV-type microseisms observed in this work might be caused by the motional induction effect.

We also simulate electromagnetic signals (Gao, 2010) generated by an earthquake source due to that geomagnetic pulsations can be also triggered by ground motion based on the electrokinetic effect (Haartsen & Pride, 1997). The magnetic field induced by a P-SV-type wave has no vertical component, because P-SV-type

waves are resulted from the interference between P and SV waves both of which produce only horizontal magnetic disturbances (Figure S7). In this work, the geomagnetic pulsations accompanying the P-SV-type waves appear on both the horizontal components and the vertical component (i.e., the elliptical rotation in Figure 6). The disagreement in the vertical induced geomagnetic field between the observed data and the electrokinetic modeling suggests that the observed geomagnetic pulsations were not likely caused by the electrokinetic effect.

It should be mentioned that there is another mechanism associated with the geomagnetic field. It is the so-called "seismic dynamo effect" proposed by Honkura and his coauthors (Honkura et al., 2009; Kuriki et al., 2011; Matsushima et al., 2013) and caused by the motion and resonance of groundwater ions in the geomagnetic field. Honkura et al. (2009) presented a theoretical model to estimate the electric field and found that a circular polarized electric field can be generated due to such a mechanism, agreeing with their observations. However, because their study did not calculate the magnetic responses, it is unknown whether such a mechanism can result in a magnetic field. This effect will need to be further explored in future studies.

In short, magnetic field generation by the motional induction effect has been confirmed (Gao et al., 2014, 2019; Yamazaki, 2012). The geomagnetic pulsations associated with such electric currents flowing in the Earth's crust should exist. The geomagnetic pulsations excited by P-SV-type microseisms based on the motional induction effect should be a common phenomenon in the world and are detectable particularly in a place over relatively high conductivity materials. However, the microseisms usually possess larger energy for the seismic stations located along the coast. Their energy could be attenuated with regard to the distance from the coast. Therefore, similar observation may not be clear for the stations located far from the coast.

5. Conclusion

The geomagnetic field is affected not only by the induced field triggered by the motion of high-conductivity seawater but also by microseisms caused by the coupling between ocean waves and the seafloor. The geomagnetic pulsations observed at the northern end of Taiwan, at the frequency band between the 0.1–0.2 Hz, are dominantly influenced by P-SV-type microseisms that propagate with a velocity of ~2.9 km/s. The absence of a significant time difference between the geomagnetic pulsations and ground motion suggests that the observed geomagnetic pulsations are triggered by microseisms. These pulsations are not directly induced by ocean waves; instead, the 90° phase difference observed on the EW component is induced by ground motion relative to the geomagnetic pulsations and on the vertical component in the magnetic pulsations. These results suggest that the geomagnetic pulsations observed in this study are likely attributed to the motional induction effect triggered by P-SV-type microseisms.

Data Availability Statement

The data utilized in this study can be downloaded at https://datadryad.org/stash/share/mfNUYpxXFCfNQsR0dx3UXCF4uId9Ps6kh_GsiirUTKk.

References

Ardhuin, F., Stutzmann, E., Schimmel, M., & Mangeney, A. (2011). Ocean wave sources of seismic noise. *Journal of Geophysical Research*, *166*, C09004. https://doi.org/10.1029/2011JC006952

Artru, J., Farges, T., & Lognonné, P. (2004). Acoustic waves generated from seismic surface waves: Propagation properties determined from Doppler sounding observations and normal-mode modeling. *Geophysical Journal International*, *158*, 1067–1077. https://doi.org/10.1111/j.1365-246X.2004.02377

Bordes, C., Jouniaux, L., Garambois, S., Dietrich, M., Pozzi, J. P., & Gaffet, S. (2008). Evidence of the theoretically predicted seismo-magnetic conversion. *Geophysical Journal International*, *174*(2), 489–504. https://doi.org/10.1111/j.1365-246X.2008.03828.x

Breiner, S. (1964). Piezomagnetic effect at the time of local earthquakes. *Nature*, *202*, 790–791. https://doi.org/10.1038/202790a0

Capon, J. (1969). High-resolution frequency-wavenumber spectrum analysis. *Proceedings of the IEEE*, *57*, 1408–1419. https://doi.org/10.1109/PROC.1969.7278

Cessaro, R. K. (1994). Sources of primary and secondary microseisms. *Bulletin of the Seismological Society of America*, *84*(1), 142–148.

Chapman, S., & Bartels, J. (1940). *Geomagnetism, vol. I: Geomagnetic and related phenomena, vol. II: Analysis of data and physical theories*. Oxford, Landon: Oxford University Press.

Chen, C. H. (1978). Petrochemistry and origin of Pleistocene volcanic rocks from northern Taiwan. *Bulletin of Volcanology*, *41*, 513–528. https://doi.org/10.1007/BF02597384

Chen, C. H., Lin, C. H., Yen, H. Y., Chen, C. R., Jan, J. C., Wang, C. H., et al. (2017). Artificial Magnetic Disturbance from the Mass Rapid Transit System in Taiwan. *Terra Nova*, *29*(5), 306–311. https://doi.org/10.1111/ter.12277

Chen, C. H., Wang, C. H., Lin, L. C., Hsieh, H. H., Yen, H. Y., & Shih, M. H. (2014). Typhoon-induced magnetic disturbances: Cases in the Western Pacific. *Terrestrial, Atmospheric and Oceanic Sciences*, *25*, 647–653. https://doi.org/10.3319/TAO.2014.05.08.01(AA)

Chen, C. S. (2008). *Investigation and monitoring of underground magma chamber of the datun volcano group: Magnetotelluric survey method*. Taiwan: Yangmingshan National Park Headquarters.

Chen, Y.-N., Gung, Y., You, S.-H., Hung, S.-H., Chiao, L.-Y., Huang, T.-Y., et al. (2011). Characteristics of short period secondary microseisms (SPSM) in Taiwan: The influence of shallow ocean strait on SPSM. *Geophysical Research Letters*, *38*, L04305. https://doi.org/10.1029/2010GL046290

Christensen, N. I., & Mooney, W. D. (1995). Seismic velocity structure and composition of the continental crust: A global view. *Journal of Geophysical Research*, *I00*, 9761–9788. https://doi.org/10.1029/95JB00259

Cooper, G. R. J., & Cowan, D. R. (2008). Comparing Time Series using Wavelet Based Semblance Analysis. *Computers and Geosciences*, *34*(2), 95–102. https://doi.org/10.1016/j.cageo.2007.03.009

Eleman, F. (1965). The response of magnetic instruments to earthquake waves. *Journal of Geomagnetism and Geoelectricity*, *18*, 43–72. https://doi.org/10.5636/jgg.18.43

Gao, Y. (2010). *Simulation of earthquake-induced electromagnetic wavefield due to the electrokinetic effect*. Harbin, China: Ph.d thesis, Harbin Institute of Technology.

Gao, Y., Chen, X., Hu, H., Wen, J., Tang, J., & Fang, G. (2014). Induced electromagnetic field by seismic waves in Earth's magnetic field. *Journal of Geophysical Research: Solid Earth*, *119*, 5651–5685. https://doi.org/10.1002/2014JB010962

Gao, Y., Harris, J. M., Wen, J., Huang, Y., Twardzik, C., Chen, X., et al. (2016). Modeling of the coseismic electromagnetic fields observed during the 2004 M-w 6.0 Parkfield earthquake. *Geophysical Research Letters*, *43*(2), 620–627. https://doi.org/10.1002/2015gl067183

Gao, Y., & Hu, H. (2010). Seismoelectromagnetic waves radiated by a double couple source in a saturated porous medium. *Geophysical Journal International*, *181*, 873–896. https://doi.org/10.1111/j.1365-246X.2010.04526.x

Gao, Y., Wang, D., Wen, J., Hu, H., Chen, X., & Yao, C. (2019). Electromagnetic responses to an earthquake source due to the motional induction effect in a 2D layered model. *Geophysical Journal International*, *219*, 563–593. https://doi.org/10.1093/gji/ggz303

Garambois, S., & Dietrich, M. (2002). Full waveform numerical simulations of seismoelectromagnetic wave conversions in fluid-saturated stratified porous media. *Journal of Geophysical Research*, *107*(B7), 2148. https://doi.org/10.1029/2001JB000316

Gilman, D. L., Fuglister, F. J., & Mitchel, J. M., Jr (1963). On the power spectrum of red noise. *Journal of the Atmospheric Sciences*, *20*(2), 182–184. https://doi.org/10.1175/1520-0469(1963)020<0182:OTPSON>2.0.CO;2

Goldstein, P., & Archuleta, R. J. (1991a). Deterministic frequency-wavenumber methods and direct measurements of rupture propagation during earthquakes using a dense array: Theory and methods. *Journal of Geophysical Research*, *96*, 6173–6185. https://doi.org/10.1029/90JB02123

Goldstein, P., & Archuleta, R. J. (1991b). Deterministic frequency-wavenumber methods and direct measurements of rupture propagation during earthquakes using a dense array: Data analysis. *Journal of Geophysical Research*, *96*, 6187–6198. https://doi.org/10.1029/90JB02472

Gregori, G. P., & Lanzerotti, L. J. (1980). Geomagnetic depth sounding by induction arrow representation: A review. *Reviews of Geophysics*, *18*(1), 203–209. https://doi.org/10.1029/RG018i001p00203

Gualtieri, L., Stutzmann, E., Capdeville, Y., Farra, V., Mangeney, A., & Morelli, A. (2015). On the shaping factors of the secondary microseismic wave field. *Journal of Geophysical Research*, *120*(9), 6241–6262. https://doi.org/10.1002/2015JB012157

Guglielmi, A. V., Potapov, A. S., & Tsegmed, B. (2004). On the excitation of magnetic signals by Love waves. *Annals of Geophysics*, *47*, 171–177. https://doi.org/10.4401/ag-3269

Haartsen, M. W., & Pride, S. R. (1997). Electroseismic waves from point sources in layered media. *Journal of Geophysical Research*, *102*(B11), 24745–24769. https://doi.org/10.1029/97JB02936

Hao, Y. Q., Xiao, Z., & Zhang, D. H. (2013). Teleseismic magnetic effects (TMDs) of 2011 Tohoku earthquake. *J. Geophys. Res. Space Physics*, *118*, 3914–3923. https://doi.org/10.1002/jgra.50326

Hasselmann, K. (1963). A statistical analysis of the generation of microseisms. *Review of Geophysics*, *1*, 177–210. https://doi.org/10.1029/RG001i002p00177

Hitchman, A. P., Milligan, P. R., Lilley, F. E. M., White, A., & Heinson, G. S. (2000). The total-field geomagnetic coast effect: The CICADA97 line from deep Tasman sea to inland New South Wales. *Exploration Geophysics*, *31*, 52–57. https://doi.org/10.1071/EG00052

Honkura, Y., Ogawa, Y., Matsushima, M., Nagaoka, S., Ujihara, N., & Yamawaki, T. (2009). A model for observed circular polarized electric fields coincident with the passage of large seismic waves. *Journal of Geophysical Research*, *114*, B10103. https://doi.org/10.1029/2008JB006117

Honkura, Y., Satoh, H., & Ujihara, N. (2004). Seismic dynamo effects associated with the M7.1 earthquake of 26 May 2003 off Miyagi Prefecture and the M6.4 earthquake of 26 July 2003 in northern Miyagi Prefecture, NE Japan. *Earth Planets and Space*, *56*, 109–114. https://doi.org/10.1186/BF03353395

Kimman, W. P., Campman, X., & Trampert, J. (2012). Characteristics of seismic noise: fundamental and higher mode energy observed in the northeast of the Netherlands. *Bulletin of the Seismological Society of America*, *102*(4), 1388–1399. https://doi.org/10.1785/0120110069

Kuriki, M., Matsushima, M., Ogawa, Y., & Honkura, Y. (2011). Spectral peaks in electric field at resonance frequencies for seismically excited motion of ions in the Earth's magnetic field. *Earth Planets and Space*, *63*, 503–507. https://doi.org/10.5047/eps.2011.03.010

Liu, J. Y., Chen, C. H., Sun, Y. Y., Chen, C. H., Tsai, H. F., Yen, H. Y., et al. (2016). The vertical propagation of disturbances triggered by seismic waves of the 11 March 2011 M9.0 Tohoku earthquake over Taiwan. *Geophysical Research Letters*, *43*, 1759–1765. https://doi.org/10.1002/2015GL067487

Lognonné, P., Clévédé, E., & Kanamori, H. (1998). Computation of seismograms and atmospheric oscillations by normal-mode summation for a spherical earth model with realistic atmosphere. *Geophysical Journal International*, *135*, 388–406. https://doi.org/10.1046/j.1365-246X.1998.00665.x

Longuet-Higgins, H. (1950a). Some studies in molecular orbital theory I. Resonance structures and molecular orbitals in unsaturated hydrocarbons. *The Journal of Chemical Physics*, *18*(3), 265–274. https://doi.org/10.1063/1.1747618

Longuet-Higgins, M. (1950b). Theory on the origin of microseisms. *Philosophical Transactions of the Royal Society of London, Series A*, *243*, 1–35. https://doi.org/10.1098/rsta.1950.0012

Matsushima, M., Honkura, Y., Kuriki, M., & Ogawa, Y. (2013). Circularly polarized electric fields associated with seismic waves generated by blasting. *Geophysical Journal International*, *194*, 200–211. https://doi.org/10.1093/gji/ggt110

Occhipinti, G., Coïsson, P., Makela, J. J., Allgeyer, S., Kherani, A., Hébert, H., & Lognonné, P. (2011). Three-dimensional numerical modeling of tsunami-related internal gravity waves in the Hawaiian atmosphere. *Earth Planets Space*, *63*, 847–851. https://doi.org/10.5047/eps.2011.06.051

Occhipinti, G., Dorey, P., Farges, T., & Lognonné, P. (2010). Nostradamus: The radar that wanted to be a seismometer. *Geophysical Research Letters*, *37*, L18104. https://doi.org/10.1029/2010GL044009

Parkinson, W. D., & Jones, F. W. (1979). The geomagnetic coast effect. *Reviews of Geophysics and Space Physics*, *17*, 1999–2015. https://doi.org/10.1029/RG017i008p01999

Pride, S. R. (1994). Governing Equations for the Coupled Electromagnetics and Acoustics of Porous-Media. *Physical Review B: Condensed Matter*, *50*(21), 15678–15696. https://doi.org/10.1103/PhysRevB.50.15678

Pu, H. C., Lin, C. H., Lai, Y. C., Shih, M. H., Chang, L. C., Lee, H. F., et al. (2020). Active Volcanism Revealed from a Seismicity Conduit in the Long-resting Tatun Volcano Group of Northern Taiwan. *Scientific Reports*, *10*(1), 6153. https://doi.org/10.1038/s41598-020-63270-7

Ren, H., Wen, J., Huang, Q., & Chen, X. (2015). Electrokinetic effect combined with surface-charge assumption: A possible generation mechanism of coseismic EM signals. *Geophysical Journal International*, *200*(2), 835–848. https://doi.org/10.1093/gji/ggu435

Revil, A., & Linde, N. (2006). Chemico-electromechanical coupling in microporous media. *Journal of Colloid and Interface Science*, *302*(2), 682–694. https://doi.org/10.1016/J.JCIS.2006.06.051

Riahi, N., Bokelmann, G., Sala, P., & Saenger, E. H. (2014). Time-lapse analysis of ambient surface wave anisotropy: A three-component array study above an underground gas storage. *Journal of Geophysical Research*, *118*, 5339–5351. https://doi.org/10.1002/jgrb.50375

Riahi, N., & Saenger, E. H. (2013). Rayleigh and Love wave anisotropy in Southern California using seismic noise. *Geophysical Research Letters*, *41*, 363–369. https://doi.org/10.1002/2013GL058518

Rolland, L. M., Lognonné, P., Astafyeva, E., Kherani, E. A., Kobayashi, N., Mann, M., et al. (2011). The resonant response of the ionosphere imaged after the 2011 off the Pacific coast of Tohoku earthquake. *Earth Planets and Space*, *63*, 853–857. https://doi.org/10.5047/eps.2011.06.020

Schisselé, E., Guilbert, J., Gaffet, S., & Cansi, Y. (2004). Accurate time-frequency-wavenumber analysis to study coda waves. *Geophysical Journal International*, *158*, 577–591. https://doi.org/10.1111/j.1365-246X.2004.02211.x

Schulz, M., & Mudelsee, M. (2002). REDFIT: Estimating red-noise spectra directly from unevenly spaced paleoclimatic time series. *Computers and Geosciences*, *28*(3), 421–426. https://doi.org/10.1016/S0098-3004(01)00044-9

Shapiro, N. M., & Camille, M. (2004). Emergence of broadband Rayleigh waves from correlations of the ambient seismic noise. *Geophysical Research Letters*, *31*, L07614. https://doi.org/10.1029/2004GL019491

Shellnutt, J. G. (2014). The Emeishan large igneous province: A synthesis. *Geoscience Frontiers*, *5*, 369–394. https://doi.org/10.1016/j.gsf.2013.07.003

Slabaugh, G. G. (1999). *Computing Euler angles from a rotation matrix*. Technical Report. London: City University http://www.gregslabaugh.net/publications/euler.pdf

Smith, Z., Murtagh, W., & Smithtro, C. (2004). Relationship between solar wind low-energy energetic ion enhancements and large geomagnetic storms. *Journal of Geophysical Research*, *109*, A01110. https://doi.org/10.1029/2003JA010044

Snieder, R. (2004). Extracting the Green's function from the correlation ofcoda waves: A derivation based on stationary phase. *Physical Review E - Statistical Physics, Plasmas, Fluids, and Related Interdisciplinary Topics*, *69*, 046610. https://doi.org/10.1103/PhysRevE.69.046610

Tsegmed, B., Guglielmi, A. V., & Potapov, A. S. (2000). Application of the polarization method to the observation of seismomagnetic waves produced by strong earthquakes. *Izvestiya - Physics of the Solid Earth*, *36*, 1021–1030.

Vassiliadis, D. V., Sharma, A. S., Eastman, T. E., & Papadopoulos, K. (1990). Low-dimensional chaos in magnetospheric activity from AE time series. *Geophysical Research Letters*, *17*, 1841–1844. https://doi.org/10.1029/GL017i011p01841

Weaver, R. L., & Lobkis, O. I. (2001). On the emergence of the Green's function in the correlations of a diffuse field. *Journal of the Acoustical Society of America*, *110*, 3011–3017. https://doi.org/10.1121/1.1417528

Weaver, R. L., & Lobkis, O. (2002). On the emergence of the Green's function in the correlations of a diffuse field: Pulse-echo using thermal phonons. *Ultrasonics*, *40*, 435–439. https://doi.org/10.1016/S0041-624X(02)00156-7

Yamazaki, K. (2012). Estimation of temporal variations in the magnetic field arising from the motional induction that accompanies seismic waves at a large distance from the epicenter. *Geophysical Journal International*, *190*, 1393–1403. https://doi.org/10.1111/j.1365-246X.2012.05586.x